

γ -Alumina Nanotubes Prepared by Hydrothermal Method as Support of Iron, Cobalt and Nickel for Fischer-Tropsch Catalysts

Dahlan¹, I Nyoman Marsih^{1*}, IGBN Makertihartha², Piyasan Prasertdam³, Joongjai Panpranot³, Ismunandar¹

1. Physical and Inorganic Chemistry Division, Faculty of Mathematic and Natural Sciences, Institute of Technology Bandung, 10 Ganesha St, Bandung 40132, Indonesia
2. Department of Chemical Engineering, Faculty of Industrial Engineering, Institute of Technology Bandung, 10 Ganesha St, Bandung 40132, Indonesia
3. Center of Excellence on Catalysis and Catalytic Reaction Engineering, Department of Chemical Engineering, Chulalongkorn University, 254 Phayathai Road, Bangkok 10330, Thailand

*E-mail of the corresponding author: nyoman@chem.itb.ac.id

Abstract

γ -Alumina nanotubes have been synthesized by hydrothermal method from aluminium nitrate nonahydrate, CTAB, urea, and water with a molar ratio of 29:153:1:2028. The alumina has BET surface area of 203.73 m²/g, pore volume of 0.14 ml/g, and average pore diameter of 2.78 nm. The crystallite size calculated by Scherer equation was in the range of 9.8–11 nm. It has been employed as support of iron, cobalt, and nickel for Fischer-Tropsch synthesis catalyst. The three catalysts were prepared by incipient wetness impregnation method. It was found that they showed different catalytic behaviours and activity. The acidity of catalysts increased according to the order: Co/Al₂O₃<Fe/Al₂O₃<Ni/Al₂O₃. The reducibility, amount of active site and catalytic activity increased in the following order: Fe/Al₂O₃<Co/Al₂O₃<Ni/Al₂O₃.

Keywords: alumina nanotubes, hydrothermal method, iron, cobalt, nickel, Fischer-Tropsch catalyst.

1. Introduction

Due to depletion of oil reserves, increased cost of petroleum, and environmental demands for clean fuels, alternative methods for synthesizing hydrocarbon fuels such as Fischer-Tropsch synthesis (FTS) have again received considerable attention and become subject of many investigations both in academic and industrial research laboratories. FTS can produce clean fuels and chemicals from syngas (mixture of H₂ and CO) which can be generated from coal, natural gas and biomass (Girardon *et al.*, 2007). It is a heterogeneously catalyzed reaction occurring at temperature $\geq 200^\circ\text{C}$ and pressure ≥ 1 atm to give paraffins as the main products based on the following equation (Philippe *et al.*, 2009):



In the FTS process, the catalytic conversion of syngas over a catalyst is considered a crucial step (de la Osa *et al.*, 2011). As a consequence, choosing a suitable catalyst is very important. Most VIII group metals have measurable activity in carbon monoxide hydrogenation. Among them, iron, cobalt, and nickel present high activity and they are economically the cheapest. The three metals have different activity, selectivity, and stability (Perego, 2007). Iron catalyst has lower CH₄ selectivity, higher selectivity to olefins and produces a high amount of oxygenates. Cobalt catalyst has a higher conversion, very good selectivity to long chain paraffin, low selectivity to oxygenates and olefin, and it is resistant to deactivation. Nickel has a very high hydrogenation activity, so its selectivity to methane is higher.

To maximize the exposure of metals to gaseous reactant and thus increasing catalytic activity as well as stability, the metals are normally dispersed on a high surface area of support ranging from metal oxides to zeolites (Idem *et al.*, 2000). The optimum support should be chemically inert, with high surface area, with good mechanical and thermal resistance. Due to high surface area and highest mechanical and thermal stability, γ -Al₂O₃ is considered as one of the most promising support (Oh *et al.*, 2009). Aluminas with various morphology have been applied as support of Fischer-Tropsch catalysts (Martinez *et al.*, 2009; Pansanga *et al.*, 2007). In line with development of synthesis methods, application of novel aluminas is of great interest.

In the field of material chemistry, recently, considerable efforts have been directed towards preparation of nanostructured alumina due to its novel properties such as high elastic modulus, thermal and chemical stability, and optical characteristic. Up to date, nanostructured alumina with different morphologies, such as nanotubes,

nanowires, nanobelts, nanofibers, rod-shaped nanoparticle, whiskers, and nanoleaves have been synthesized by a variety of routes (Qu *et al.*, 2005). Based on the unique electronic, mechanical and chemical properties of carbon nanotubes with marked shape-specific and quantum size effect, nanotubular materials are expected to exhibit both unusual characteristics and potential applications (Baughman, *et al.*, 2002). To prepare alumina nanotubes, many efforts have been made via different methods inclusive of hydrothermal treatments on aluminium precursor in the presence of surfactants (Cheng, *et al.*, 2006; Liu *et al.*, 2008; Lu *et al.*, 2009). This methods avoids the use of organic solvents and allows the synthesis of boehmite precursor of γ -Al₂O₃ at lower temperature.

In this work we synthesized γ -Al₂O₃ by the hydrothermal method using aluminium nitrate nonahydrate as aluminium precursor and CTAB as surfactant. The alumina was used as support of iron, cobalt, and nickel for Fischer-Tropsch catalyst. To the best of our knowledge, the three metals have never been investigated in the same conditions including preparation methods, support, metal loading, and catalytic test. To acquire a powerful and reliable conclusion on comparison of their catalytic behaviours and activity, we applied the same treatments to these catalysts from preparation to catalytic test.

2. Experimental

2.1 Preparation of γ -Al₂O₃

The γ -Al₂O₃ was prepared through hydrothermal process previously reported by Cheng *et al.* (2006) with modifications in starting materials, molar ratio, and calcination temperature. The starting materials consisting of Al(NO₃)₃·9H₂O, urea, CTAB (all obtained from Aldrich) and deionized water were mixed at a molar ratio of 29:153:1:2028 and magnetic stirred to obtain a transparent solution. The solution was transferred into a 100 ml Teflon autoclave and then it was heated at 125 °C and kept at that temperature under autogenous pressure. After 15 h, the autoclave was cooled to room temperature naturally. White precipitate formed was collected by filtration, washed with ethanol and then dried in air at 120 °C for 12 h. Afterwards the product was calcined in a muffle furnace by heating up to 550 °C for 3.5 h.

2.2 Preparation of Al₂O₃-Supported Catalysts

The 15%Fe/Al₂O₃, 15%Co/Al₂O₃, and 15%Ni/Al₂O₃ catalysts were prepared by incipient wetness impregnation method. Fe(NO₃)₃·9H₂O, Co(NO₃)₂·6H₂O, and Ni(NO₃)₂·9H₂O (all from Aldrich) were used as source of Fe, Co, and Ni respectively. A desired amount of aqueous solution of nitrate salt was added dropwise to Al₂O₃ and simultaneously stirred to obtain a homogenous mixture. The samples were dried at 110 °C for 24 h and calcined at 450 °C for 3 h.

2.3 Characterization

XRD patterns of the samples were collected with Philips Analytical PW1710 X-ray diffractometer with Cu K α radiation (λ = 1.54439 Å). The spectra were scanned at a rate of 0.02°/step from 2θ = 10° to 90°. BET surface areas were measured by NOVA 1000 Gas Sorption Analyzer Version 3.70 at liquid N₂ temperature. SEM and EDX were performed with JEOL JSM 6063LA in the back scattering electron (BSE) mode at 10 kV. AAS for measurement of metal loading on catalysts were carried out by Shimadzu AA-630-12. H₂-TPR, NH₃-TPD, and H₂ chemisorption were done with Micromeritics Chemisorb 2750 system. For H₂-TPR, a temperature ramp from 35 to 800 °C at a ramp rate 10 °C/min and reduction gas 10% H₂ in Ar were used. A thermal conductivity detector (TCD) was used to determine the amount of hydrogen consumed. For NH₃-TPD, samples were pretreated under He flow at 500 °C for 2 h before NH₃ adsorption at 100 °C. TPD profiles were recorded from 35 to 500 °C under He flow at heating rate of 10 °C/min. Static H₂ chemisorption was carried out on the reduced catalyst samples at 100 °C. Prior to H₂ chemisorption, the catalyst samples were reduced at 400 °C in flowing H₂ for 3 h.

2.4 Catalytic Test

Catalytic test in Fischer-Tropsch synthesis was done in a quartz tubular microreactor of 6 mm internal diameter. Typically, 0.2 g of catalyst sampel was placed into microreactor and then it was reduced in flowing H₂ (7 ml/min) at atmospheric pressure and temperature of 400°C for 3 h. Afterwards the temperature was reduced to

200°C and catalyst was fed with syngas of ratio $H_2/CO=2$ and flow rate of 7 ml/min. After 1 h, the product of reaction was taken and analyzed offline by GC Shimadzu 8A to determine the concentration of CO. CO conversion was calculated according to equation:

$$\text{CO conversion} = \frac{[\text{CO}]_{\text{in}} - [\text{CO}]_{\text{out}}}{[\text{CO}]_{\text{in}}} \times 100\% \quad (2)$$

3. Result and Discussion

3.1 Properties of Alumina and Catalysts

Product of the synthesis was alumina powder. The alumina was formed through boehmite ($\gamma\text{-AlOOH}$) resulted from hydrolysis of aluminium precursor under hydrothermal treatment. After calcination, $\gamma\text{-AlOOH}$ was dehydrated and transformed into $\gamma\text{-Al}_2\text{O}_3$ (Liu *et al.*, 2008; Lu *et al.*, 2009).



The gamma phase of alumina was confirmed by XRD pattern characteristic of $\gamma\text{-Al}_2\text{O}_3$ (ICDD No. 10-0425). As shown in Figure 1(a), there are six main peaks of $\gamma\text{-Al}_2\text{O}_3$ at 2θ 37.84°, 39.54°, 45.88°, 61.32°, 67°, and 85°. All peaks can be indexed to a cubic unit cell of $\gamma\text{-Al}_2\text{O}_3$ ($a=b=c=7.90 \text{ \AA}$), space group symmetry of $Fd\bar{3}m(227)$. It is very clear that alumina particles show nano-size nature as indicated by broadened peaks due to presence of small crystallite sizes. The crystallite size was calculated by using Scherrer equation (Potdar *et al.*, 2007). It was found to be in the range of 9.8–11 nm.

The calcination of metal precursors in air led to formation of their oxides, namely Fe_2O_3 , Co_3O_4 , and NiO on alumina. The existence of these oxides is very obvious by the emergence of new peaks in XRD pattern of impregnated alumina corresponding to Fe_2O_3 (ICDD No. 84-0311), Co_3O_4 (ICDD No. 43-1003), and NiO (ICDD No. 44-1159). Figure 1(c) shows two peaks of Fe_2O_3 emerging at 2θ 33.42° and 35.62°. The low intensity and broad diffraction peaks implies low crystallinity or small crystallite size of Fe_2O_3 . Figure 1(d) exhibits five peaks of Co_3O_4 at 2θ 31.3°, 36.75°, 44.82°, 59.56°, and 65.2°. Figure 1(b) shows five peaks of NiO at 2θ 37.06°, 43.18°, 62.6°, 75.05°, and 79.54°. The diffraction peaks of NiO are sharper than those Fe_2O_3 and Co_3O_4 indicating a characteristic of larger NiO crystallite. Thus, the XRD pattern suggests that the metal oxides have different crystallite size in the order: $\text{Fe}_2\text{O}_3 < \text{Co}_3\text{O}_4 < \text{NiO}$. This can be attributed to the difference in metal oxide-support interaction (Zhang *et al.*, 2006). Large crystallite results from aggregation of metal oxide particles due to weak metal oxide-support interaction. On the contrary, strong interaction prevents the aggregation leading to formation of small metal oxide crystallite. Therefore, it implies that the order in strength of interaction with alumina is $\text{NiO} < \text{Co}_3\text{O}_4 < \text{Fe}_2\text{O}_3$.

As shown in Figure 2, the alumina exhibited a uniform morphology of nanotubes. The formation of nanotubes is induced by the micelles of surfactant as soft template (Diniz *et al.*, 2007). The addition of CTAB is critical for the production of uniform morphology. It was reported that without using the surfactant in the similar synthetic system, only particles with random size and morphology distribution were obtained (Music *et al.*, 1999). A slight change of alumina morphology occurred after addition of metal oxides. SEM micrograph of the three catalysts showed a difference in density of surface morphology. This may be correlated to the amount of metal oxides on the alumina since the EDX data also presented a difference in metal concentration as shown in Table 1. Ni/ Al_2O_3 catalyst has the densest surface morphology as well as the highest metal composition.

As shown in Table 1, elemental composition of alumina displayed by EDX data were in good agreement with calculated value showing that the alumina has no impurities. Unlike alumina, the catalysts were not homogenous solids since metal oxides particles were not evenly distributed on alumina. As will be explained later, the metal oxides mostly existed in the pores of alumina. Therefore, metal composition displayed by EDX taken from a small spot of catalyst sample was not reliable for metal loading on catalyst and it was confirmed by AAS. The higher metal composition shown by EDX data especially in Ni/ Al_2O_3 catalyst showed that the spot shot was rich in metal oxide. Impregnation efficiency were below 100% as according to AAS data, metal concentration in calcined catalyst samples were lower than calculated values corresponding to 15% wt metal in reduced catalysts. There impregnation efficiency in Fe/ Al_2O_3 , Co/ Al_2O_3 , and Ni/ Al_2O_3 were 88%, 84%, and 92% respectively.

As shown in Table 2, the alumina has surface area of 203.73 m²/g, pore volume of 0.14 ml/g and average pore diameter of 2.78 nm. There was a significant decrease in surface area and pore volume upon the presence of metal oxides. The metal concentration values of 12.38% Fe, 11.9% Co, and 13.26% Ni from AAS are equivalent to percentage by weight of 18% Fe₂O₃, 16% Co₃O₄, and 17% NiO respectively. If the Al₂O₃ was the only contributor to the area, then the area of Fe/Al₂O₃ catalyst at least should be 0.82 x 203.73 m²/g = 167 m²/g. The minimum area of Co/Al₂O₃ catalyst should be 0.84 x 203.73 m²/g = 171.13 m²/g and that of Ni/Al₂O₃ catalyst should be 0.83 x 203.73 m²/g = 169 m²/g. However, all catalysts presented lower surface area value suggesting additional pore blockage by metal oxide clusters (de la Osa *et al.*, 2011). This effect was more pronounced in Ni/Al₂O₃ catalyst due to larger crystallite size of NiO as has been seen from XRD pattern. The large crystallites fill up more space in the pore causing larger decrease in surface area. The alumina might be the main contributor to pore volume of catalysts. Percentage values of surface area reduction and pore volume reduction were almost the same confirming that metal oxides particle were mainly incorporated inside the pores rather than on the external surface of alumina.

3.2 Catalytic Behaviours and Activity

The catalysts acidity were measured by temperature-programmed desorption (TPD). Due to acidic nature of catalysts surface, they adsorbed ammonia as a basic compound at low temperature and then desorbed it at higher temperature. The temperature of ammonia desorption depends on the acidity of the catalyst. TPD profile in Figure 3 presented a slight difference in the temperature of ammonia desorption of the three catalysts. Fe/Al₂O₃ catalyst showed a strong desorption of ammonia at 172-252 °C. A strong desorption of ammonia by Co/Al₂O₃ catalyst occurred at temperature 104-125 °C. Ni/Al₂O₃ catalyst exhibited two peaks of desorption at 118-149 °C and 248-278 °C. The broader range of desorption shown by Ni/Al₂O₃ indicated its stronger acidic nature. Thus, the sequence of acidity of catalyst was Co/Al₂O₃ < Fe/Al₂O₃ < Ni/Al₂O₃.

Reducibility of the catalysts were studied by temperature-programmed reduction (TPR). Hydrogen is consumed in reduction of metal oxide to metal phase. Figure 4 exhibits TPR profile of the catalysts. Two peaks in the TPR profile of Fe/Al₂O₃ corresponds to two steps reduction of Fe₂O₃ to metallic iron via Fe₃O₄ (Luo *et al.*, 2009). Therefore, the first peak appeared at 372-383 °C is attributed to reduction of Fe₂O₃ to Fe₃O₄ and the second peak emerged at 593-622 °C is assigned to reduction of Fe₃O₄ to Fe. There were also two peaks in Co/Al₂O₃ catalyst resulting from two steps reduction of Co₃O₄ to cobalt metal with CoO as an intermediate species (Borg *et al.*, 2007). The first peak formed at 329-344 °C is assigned to reduction of Co₃O₄ to CoO and the second peak at 502-535 °C is attributed to reduction of CoO to Co. In Ni/Al₂O₃ catalyst, only one main peak appeared at 346-369°C corresponding to reduction of NiO to Ni.

Based on the difference in reduction temperature, it could be concluded that the sequence of reducibility of the catalysts was Fe/Al₂O₃ < Co/Al₂O₃ < Ni/Al₂O₃. Taking the ionic radii and thus the charge density of the metal cation into consideration, the order of binding energy between metal and oxygen in the oxides is NiO < Fe₂O₃ < Co₃O₄. It seems that the highest reducibility of NiO is correlated with the lowest binding energy of nickel and oxygen atom. Despite the lower in binding energy between metal and oxygen, Fe₂O₃ was less reducible than Co₃O₄. This might result from stronger iron-alumina interaction as has been explained from XRD pattern.

Although a lot of metal atoms exist on catalyst after reduction step, only the metal atoms on the surface are active for CO hydrogenation. Therefore, the catalytic activity depends on the amount of surface metal as active site. The amount of active site on the catalyst sample was calculated from H₂ chemisorption experiment at 100 °C. It was equal to two times the amount of H₂ adsorbed. The result showed that the trend in the amount of active site was similar to reducibility. The higher the reducibility, the higher the total amount of metal formed from metal oxides, and consequently, the higher the amount of active site. Ni/Al₂O₃ catalyst has much more active sites than Fe/Al₂O₃ and Co/Al₂O₃ catalysts. This is not surprising as it is obvious from TPR profile that Ni/Al₂O₃ catalyst can be completely reduced at reduction temperature of 400 °C. The small amount of active sites in Fe/Al₂O₃ and Co/Al₂O₃ indicated that only a fraction of Fe₂O₃ and Co₃O₄ were reduced after the reduction step. As shown in Table 3, the CO conversion was in accord with the amount of active site. The activity of catalysts increased according to the order: Fe/Al₂O₃ < Co/Al₂O₃ < Ni/Al₂O₃.

4. Conclusion

Hydrothermal synthesis of alumina using Al(NO₃)₃·9H₂O as aluminium precursor and CTAB as surfactant in this research resulted in γ-Al₂O₃ nanotubes with high surface area. The alumina have been applied as support of

iron, cobalt, and nickel for Fischer-Tropsch catalyst. The three metal oxides have different strength of interaction with alumina leading to difference crystallite size of the metal oxides which have impact on catalysts surface area. The catalysts acidity increased in the following order: $\text{Co}/\text{Al}_2\text{O}_3 < \text{Fe}/\text{Al}_2\text{O}_3 < \text{Ni}/\text{Al}_2\text{O}_3$. The catalysts reducibility increased according to the order: $\text{Fe}/\text{Al}_2\text{O}_3 < \text{Co}/\text{Al}_2\text{O}_3 < \text{Ni}/\text{Al}_2\text{O}_3$. The catalysts reducibility is affected by the binding energy between metal and oxygen in their oxides and interaction between metal and support. As a consequence of reducibility, the amount of active sites and the catalytic activity in CO hydrogenation increased according to the order: $\text{Fe}/\text{Al}_2\text{O}_3 < \text{Co}/\text{Al}_2\text{O}_3 < \text{Ni}/\text{Al}_2\text{O}_3$.

Acknowledgements

The authors are grateful to ITB Institute of Research and Community Services as well as I-MHERE Implementing Unit for financial support of this research.

References

- Baughman, R. H., Zakhidov, A. A., & de Heer, W. A. (2002), "Carbon nanotubes – the route towards applications", *Science*, **297**, 787-792.
- Borg, Ø., Sigrid, E., Blekkan, E. A., Storsæter, S., Wigum, H., Rytter, E., & Holmen, A. (2007), "Fischer-Tropsch synthesis over γ -alumina-supported cobalt catalysts: Effect of support variables", *Journal of Catalysis*, **248**, 89-100.
- Cheng, B., Qu, S., Zhou, H., & Wang, Z. (2006), " $\text{Al}_2\text{O}_3:\text{Cr}^{3+}$ nanotubes synthesized via homogenization precipitation followed by heat treatment", *Journal of Physical Chemistry B*, **110**, 15749-15754.
- de la Osa, A. R., de Lucas, A., Romero, A., Valverde, J. L., & Sánchez, P. (2011), "Fischer-Tropsch diesel production over calcium-promoted Co/alumina catalysts: Effect of reaction conditions", *Fuel*, **90**, 1935-1945.
- Diniz, C. F., Balzuweit, K., & Mohallem, N. D. S. (2007), "Alumina nanotubes: preparation and textural, structural and morphological characterization", *Journal of Nanoparticle Research*, **9**, 293-300.
- Girardon, J. S., Quinet, E., Griboval-Constant, A., Chernavskii, P. A., Gengembre, L., & Khodakov, A. Y. (2007), "Cobalt dispersion, reducibility, and surface sites in promoted silica-supported Fischer-Tropsch catalysts", *Journal of Catalysis*, **248**, 143-157.
- Idem, R. O., Katikaneni, S. P. R., Sethuraman, R., & Bakhshi, N. N. (2000), "Production of C_4 hydrocarbons from modified Fischer-Tropsch Synthesis over Co-Ni-ZrO₂/sulfated- ZrO₂ hybrid catalysts", *Energy & Fuels*, **14**, 1072-1082.
- Liu, Y., Ma, D., Han, X., Bao, X., Frandsen, W., Wang, D., & Su, D. (2008), "Hydrothermal synthesis of microscale boehmite and gamma nanoleaves alumina", *Material Letter*, **62**, 1297-1301.
- Lu, C. L., Lv, J. G., Xu, L., Guo, X. F., Hou, W. H., Hu, Y., & Huang, H. (2009), "Crystalline nanotubes of γ -AlOOH and γ -Al₂O₃: hydrothermal synthesis, formation mechanism and catalytic performance", *Nanotechnology*, **20**, 215-604.
- Luo, M., Hamdeh, H., & Davis, B. H. (2009), "Fischer-Tropsch synthesis catalysts activation of low alpha iron catalyst", *Catalysis Today*, **140**, 127-134.
- Martínez, A., Prieto, G., & Rollán, J. (2009), "Nanofibrous γ -Al₂O₃ as support for Co-based Fischer-Tropsch catalysts: Pondering the relevance of diffusional and dispersion effect on catalytic performance", *Journal of Catalysis*, **263**, 292-305.
- Music, S., Dragcevic, D., Popovic, S., & Vdovic, N. (1999), "Chemical and microstructural properties of Al-oxide phases obtained from AlCl₃ solutions in alkaline medium", *Material Chemistry and Physics*, **59**, 12-19.
- Oh, J.-H., Bae, J. W., Park, S.-J., Khanna, P. K., & Jun, K.-W. (2009), "Slurry-phase Fischer-Tropsch synthesis using Co/ γ -Al₂O₃, Co/SiO₂ and Co/TiO₂: Effect of support on catalyst aggregation", *Catalysis Letter*, **130**, 403-409.
- Pansanga, K., Mekasuwandumrong, O., Panpranot, J., & Praserttham, P. (2007), "Synthesis of nanocrystalline alumina by thermal decomposition of aluminium isopropoxide in 1-butanol and their applications as cobalt catalyst support", *Korean Journal of Chemical Engineering*, **24**(3), 397-402.
- Perego, C. (2007), "Development of Fischer-Tropsch catalyst: From laboratory to commercial scale demonstration", *Rendiconti Lincei*, **18**(4), 305-317.

Philippe, R., Lacroix, M., Dreibine, L., Pham-Huu, C., David, E., Savin, S., Luck, F., & Schweich, D. (2009), "Effect of structure and thermal properties of a Fischer-Tropsch catalyst in a fixed bed", *Catalysis Today*, **147S**, S305-S312.

Potdar, H. S., Jun, K.-W., Bae, J. W., Kim, S.-M., & Lee, Y.-J. (2007), "Synthesis of nano-sized porous γ -alumina powder via a precipitation/digestion route", *Applied Catalysis A: General*, **321**, 109-116.

Qu, L., He, C., Yang, Y., He, Y., & Liu, Z. (2005), "Hydrothermal synthesis of alumina nanotubes templated by anionic surfactant", *Material Letter*, **59**, 4034-4037.

Zhang, Y., Nagamori, S., Hinchiranan, S., Vitidsant, T., & Tsubaki, N. (2006), "Promotional effects of Al_2O_3 addition to Co/SiO_2 catalysts for Fischer-Tropsch synthesis", *Energy & Fuels*, **20**(2), 417-421.

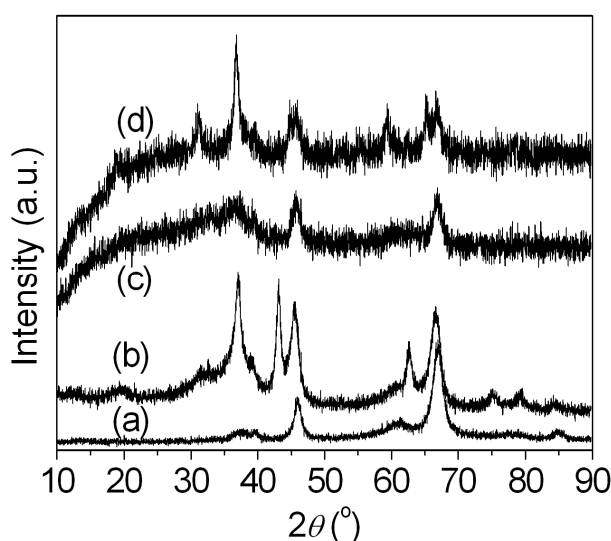


Figure 1. XRD pattern of (a) $\gamma\text{-Al}_2\text{O}_3$, (b) $\text{Ni}/\text{Al}_2\text{O}_3$, (c) $\text{Fe}/\text{Al}_2\text{O}_3$, and (d) $\text{Co}/\text{Al}_2\text{O}_3$

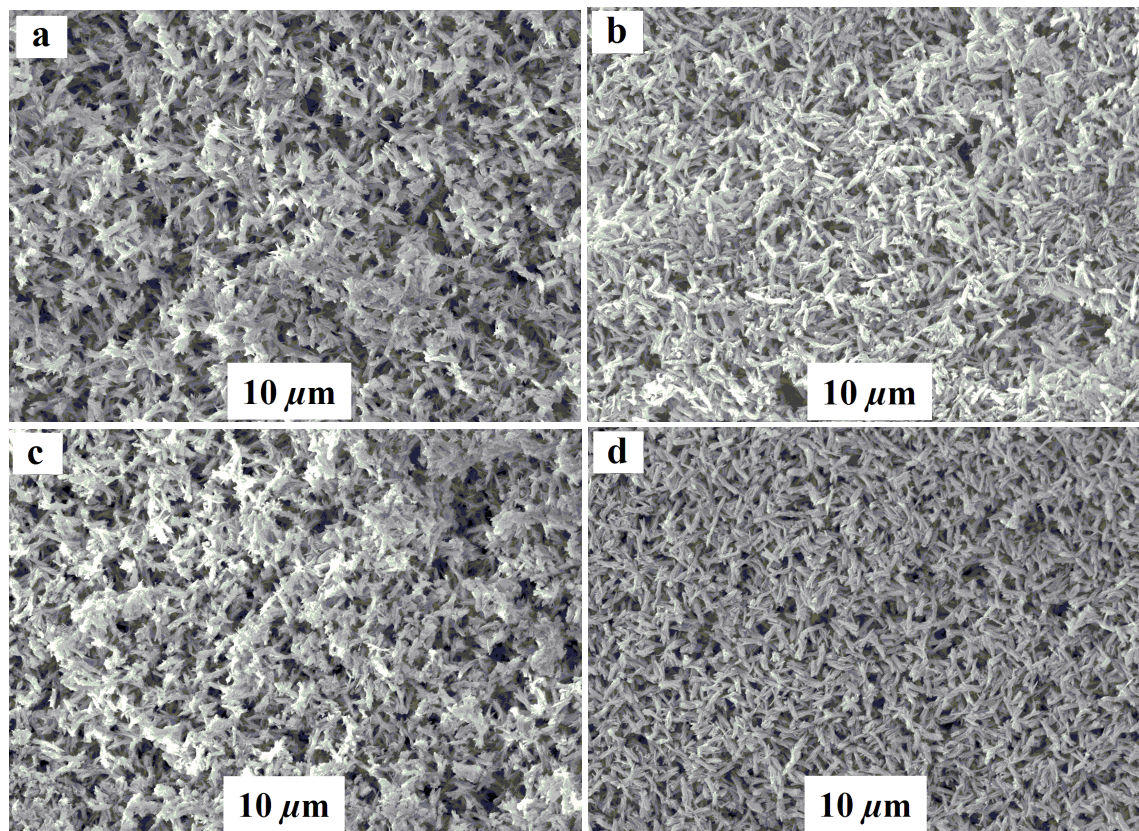


Figure 2. SEM micrograph of (a) Al_2O_3 , (b) $\text{Fe}/\text{Al}_2\text{O}_3$, (c) $\text{Co}/\text{Al}_2\text{O}_3$, and (d) $\text{Ni}/\text{Al}_2\text{O}_3$.

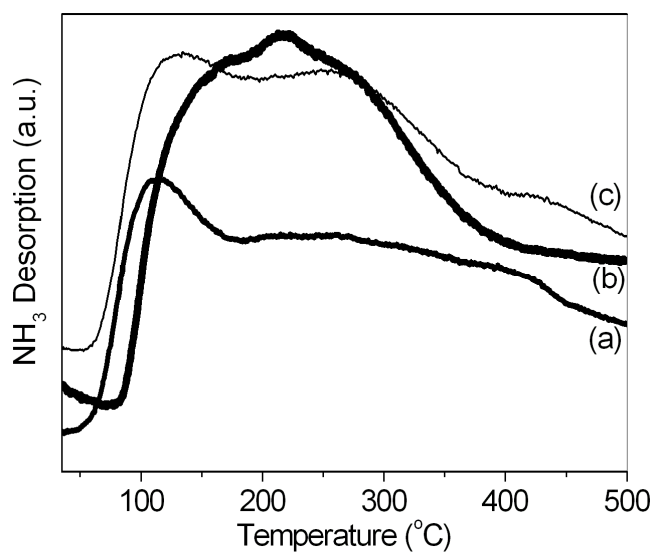


Figure 3. TPD profile of catalysts: (a) $\text{Co}/\text{Al}_2\text{O}_3$, (b) $\text{Fe}/\text{Al}_2\text{O}_3$, and (c) $\text{Ni}/\text{Al}_2\text{O}_3$

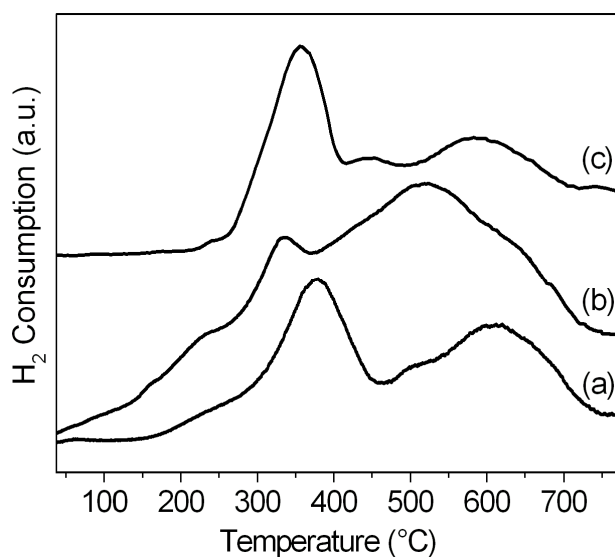


Figure 4. TPR profile of catalysts: (a) Fe/Al₂O₃, (b) Co/Al₂O₃, and (c) Ni/Al₂O₃

Table 1. Elemental composition

Support/ catalyst	Elemental composition (% wt)		
	EDX Data	AAS data	Calculated value
Al ₂ O ₃	Al = 52.93 O = 47.07	—	Al = 52.93 O = 47.07
Fe/Al ₂ O ₃	Fe = 12.92	Fe = 12.38	Fe = 14.09
Co/Al ₂ O ₃	Co = 12.24	Co = 11.9	Co = 14.24
Ni/Al ₂ O ₃	Ni = 30.49	Ni = 13.26	Ni = 14.42

Table 2. Surface area and porosity

Support/ catalyst	Surface area (m ² /g)	Δ Surface area (%)	Pore volume (ml/g)	Δ Pore volume (%)	Average pore diameter (nm)
Al ₂ O ₃	203.73	—	0.14	—	2.78
Fe/Al ₂ O ₃	120.1	41	0.08	42.8	2.83
Co/Al ₂ O ₃	135.29	33.6	0.09	35.7	2.77
Ni/Al ₂ O ₃	102.38	49.8	0.07	50	2.8

Table 3. H₂ chemisorption and CO conversion

Catalyst	H ₂ adsorbed (μmol/g cat)	Active site (μmol/g cat)	CO conversion (%)
Fe/Al ₂ O ₃	3.16	6.32	31.75
Co/Al ₂ O ₃	6.44	12.88	39.50
Ni/Al ₂ O ₃	31.72	63.44	51.03

This academic article was published by The International Institute for Science, Technology and Education (IISTE). The IISTE is a pioneer in the Open Access Publishing service based in the U.S. and Europe. The aim of the institute is Accelerating Global Knowledge Sharing.

More information about the publisher can be found in the IISTE's homepage:

<http://www.iiste.org>

The IISTE is currently hosting more than 30 peer-reviewed academic journals and collaborating with academic institutions around the world. **Prospective authors of IISTE journals can find the submission instruction on the following page:**

<http://www.iiste.org/Journals/>

The IISTE editorial team promises to review and publish all the qualified submissions in a fast manner. All the journals articles are available online to the readers all over the world without financial, legal, or technical barriers other than those inseparable from gaining access to the internet itself. Printed version of the journals is also available upon request of readers and authors.

IISTE Knowledge Sharing Partners

EBSCO, Index Copernicus, Ulrich's Periodicals Directory, JournalTOCS, PKP Open Archives Harvester, Bielefeld Academic Search Engine, Elektronische Zeitschriftenbibliothek EZB, Open J-Gate, OCLC WorldCat, Universe Digital Library, NewJour, Google Scholar

